Bull. Pharm. Sci., Assiut University, Vol. 45, Issue 1, 2022, pp. 23-40

Bulletin of Pharmaceutical Sciences
Assiut University
Website: http://bpsa.journals.ekb.eg/
e-mail: bullpharm@aun.edu.eg

BULL. PHARM. SCI. Assiut Univ.

SYNTHESIS OF ZnO NANO POWDERS USING POLYETHYLENE GLYCOL BY THE CONTROLLED MICROWAVE METHOD

A. S. Abdulhadi[1], Gamal A. Gouda[1,*], A. M. Hamed[1], M. A. Abu-Saied[2] and M.A. El-Mottaleb[1]

[1]*Department of Chemistry, Faculty of Science, Al–Azhar University, Assiut Branch, Assiut, Egypt*
[2]*Advanced Technology and New Materials Research Institute, the City of Scientific Research and Technological Applications (SRTA-City), New Borg Al-Arab, Alexandria 21934, Egypt*

Zinc oxide nanoparticles (ZnO NPs) was synthesized using some factors influencing such as the polyethylene glycol (PEG) as a stabilizing agent at different pH and temperatures. The best conditions for preparing ZnO NPs were at pH 11, 0.1 M (7.5 mL) of PEG with molecular weights of 20000 and 60 oC. Properties of synthesized ZnO NPs were confirmed using different techniques (FTIR, UV-Vis, XRD, SEM and TEM). Obviously, UV-Vis spectrum of ZnO NPs showed an adsorption peak at 268 and 362 nm with a direct bandgap of 3.39 eV. PL spectra of ZnO NPs showed an emission peak at 420 nm. The average sizes calculated of ZnO NPs powder using the XRD line broadening method were 19.71 nm. TEM observation showed that the prepared ZnO NPs is spherical with different diameters in the range 22.2-27.8 nm. Moreover, the ZnO NPs prepared have an excellent adsorption capacity for the removal of some cations from water. The adsorption capacities were 391.6 and 437.2 mg/g for Mn(II) and Cd(II) respectively. Langmuir, Freundlich and Temkin models would be well described the adsorption process. Thermodynamically, the adsorption processes of ZnO NPs were spontaneous, endothermic, and physical in nature. The good removal efficiency of Mn(II) and Cd(II) by ZnO NPs with their exceptional adsorption capability suggests that the ZnO NPs have great potential applications in environmental protection.

Keywords: *ZnO nanoparticles, polyethylene glycol, synthesis, characterization, applications.*

INTRODUCTION

Zinc oxide is a rare inorganic material in the natural environment. ZnO has been the bandgap from 3.27 eV for the single crystal to 3.55 eV for the deposited film[1&2], so it has semiconductor and piezoelectric properties. The variation in bandgap in deposited film and nanostructured of ZnO has been related to the structural morphology and defects present in the crystal[3&4]. For clinical purposes, ZnO is used potentially, it is more competent for the synthesis of nanoparticles than that of another metals[5&6]. ZnO nanoparticles can be synthesized through numerous physiochemical pathways, such as soil-gel, co-precipitation, laser vaporization, and microemulsion[7&8]. ZnO nanoparticles are widely used additives in sunscreen and cosmetics that help block ultraviolet radiation. The smaller size of these nanoparticles provides the skin with greater protection against ultraviolet damage[9]. The variety of structures of ZnO nanoparticles means that ZnO can be classified among new materials with potential applications in different fields of nanotechnology, ZnO may occur in one- (1D), two- (2D). and three-dimensional (3D) structures. Dimensional structures are the largest group, including nanorods[10&11], needles[12], -helixes, -springs and -rings[13], ribbons[14], -tubes[15], -belts[16], and -wires[17&18]. ZnO is available in 2D structures, such as nanoplates/nanosheets and nanopellets[19&20].

Received in 13/9/2021 & Accepted in 24/10/2021

*Corresponding author: Gamal A. Gouda, E-mail: ggouda73@azhar.edu.eg

Recently, significant efforts are ongoing to improve and investigate the uses of NPs in applications such as membrane isolation, sensing, catalysis, adsorption, and processing with a view to improved environmental safety[21&22]. ZnO was approved by the United States Food and Drug Administration (FDA) as a GRAS compound (generally known to be safe)[23&24]. In numerous studies, ZnO nanoparticles showed high absorption in the UV region as well as strong yellow-orange emission[25&26]. Moreover, the ZnO nanoparticles demonstrated good antibacterial activity against some organisms and a fair photocatalytic degradation of methylene blue dye pollutants. Also, the synthesized ZnO nanoparticles reveal interesting features for various potential future applications[27&28]. A major application of nanomaterials is the removal of heavy metals in water. A heavy metal can be defined as any metallic chemical element that has a relatively high density and is toxic or poisonous at low concentrations[29&30]. Their concentrations in aquatic environments have increased due to mining and industrial activities and geochemical processes[31&32]. Due to heavy metals such as Mn, Cu, Hg, Pb, Cd, etc. could pose a serious threat to human health because they can be stored biologically in the food chain[33]. For example, heavy metals can cause damage to the kidneys, mental and central nervous functions, lungs, and another organs[34&35]. Therefore, it was necessary to look for cheap nanomaterials able to remove those elements that pollute the water. Recently, several studies were carried out on low-cost natural and chemical adsorbents for the removal of some metal ions from natural resources. Zinc compounds based on nanomaterials are good adsorbents of some heavy metal ions from wastewater[36&37].

In the current work, ZnO NPs was prepared and characterized. The obtained nanoparticles of ZnO were used as a tool for the removal of selected metal ions.

Chemicals and reagents

The main chemicals and reagents used are of high grade, they are used without further purification. In all experiments, water deionized water was used to wash all glassware. Various chemicals and reagents were used in this study, as follows: Zinc (II) sulfate heptahydrate ($ZnSO_4 \cdot 7H_2O$) with a purity of 98 % was obtained from Sigma-Aldrich; Cadmium (II) chloride 2.5-hydrate ($CdCl_2 \cdot 2.5H_2O$) with a purity of 99.9 % was obtained from Wako. Manganese (II) sulfate monohydrate ($MnSO_4 \cdot H_2O$) with a purity of 99.9 %, was obtained from Morgan Chemical IND, Egypt; Polyethylene glycol (PEG) with M.wt is 1000, 6000, 8000, and 20000 was obtained from Panreac, Spain; Sodium hydroxide (NaOH) pellets (Extra pure) was obtained from Oxford.

Synthetic parameters that effect of ZnO NPs formation

Several experiments were conducted to determine the ideal conditions for the formation of ZnO NPs. The main studied factors that affected ZnO NPs morphology were: (i) The effect of pH on the reaction medium was tested at pH 7, 9, 11, and 13. (ii) Effect of added amount (at 5, 7.5, 10, and 12.5 ml) of the stabilizing agent (PEG with M.wt 20000). (iii) Effect of temperature (at 30, 40, 50 and 70 ^oC).

In the current study, ZnO NPs powder was prepared by microwave method[38&39] heating of a mixture that contains $ZnSO_4 \cdot 7H_2O$ (0.1 M) with stabilizing agent as the polyethylene glycol (PEG) and sodium hydroxide solution (NaOH) as precursors which slowly added dropwise to solutions under vigorous stirring at different temperatures of the mixture. In microwave oven the mixture was heated for 3 minutes then the precipitates were washed by distilled water and filtered. The precipitate was dried in an oven for three hours at 75 °C. The best factors effecting the synthesized of ZnO NPs such as the amount of stabilizing agent, pH, and temperature can be summarized in the following Table 1.

Table 1: The best factors for the synthesized ZnO NPs.

Type of factor	ZnO NPs
Stabilizing agent	Polyethylene glycol with M.wt is 20000
Amount of stabilizing agent	0.1 M (7.5 ml)
pH	11
Temperature	60 ℃

Characterization of synthesized ZnO NPs

All samples and chemicals for solutions preparation were weighed using an Analytical

Balance Model-220 of (Denver Instrument Co., U.S.A.) with a sensitivity of 4-10 g. The absorption was measured using a Labomed double-beam UV-visible spectrophotometer equipped with 1 cm quartz cells controlled by a PC performing the spectrophotometric. The synthesized ZnO NPs was dispersed in DMF and optical characterizations were performed. PL spectroscopy has been recorded with JASCO spectrofluorometer FP-6300. The prepared ZnO NPs was confirmed by FT-IR spectroscopy using the Thermo Fisher-model: Nicolet iS10 FT-IR spectrophotometer. The size of ZnO NPs was determined by a Philips X-ray diffractometer, PW 1710. The size and form of prepared nanomaterials were studied using scanning electron microscopy [(SEM; JEOL (JSM 5400LV)] and transmission electron microscopy [(TEM; JEOL (JEM-100 CXII)].

Adsorption process

The principal application of this study is the removal of Mn(II) and Cd(II) ions from wastewater using ZnO NPs as adsorbent by the adsorption method. The metal ions solutions were prepared by dissolving $MnSO_4 \cdot H_2O$ or $CdCl_2 \cdot 2H_2O$ in deionized water to prepare different concentrations: the initial metal concentration of Mn(II) is 500 mg/L and Cd(II) is 550 mg/L. All adsorption tests were conducted in batches using 100 ml tapered flasks at room temperature. Different parameters affecting the adsorption process were examined, including: (i) Effect of contact time; experiments are performed using 10 mL of Mn(II) and Cd(II) solution with 25 mg of prepared adsorbent ZnO NPs at pH 4.81. This system was left at various predetermined intervals at a temperature of 30 ^oC. The residual concentration of Mn(II) and Cd(II) was determined for different contact times (from 3 to 300 min). (ii) Effect of adsorbent dosage; adsorption of Mn(II) and Cd(II) ions on ZnO NPs was investigated by changing the amount of adsorbent from 0.015 to 0.25 g/L in the test solution with keeping the initial Mn(II) and Cd(II) concentrations at 500 and 550 mg/L respectively, the temperature at 30 ^oC, pH 4.82 and equilibrium time 24h. (iii) Effect of pH; the experiments performed in the pH range 1.57-7.02 keeping all other parameters constant. The solution pH was adjusted to the required value using 0.1M HNO_3 or 0.1M NaOH. pH values of the waste solutions were adjusted using a pH meter (Denver Instrument Co., U.S.A.). (iv)The effect of the temperature; the adsorption of Mn(II) and Cd(II) ions by ZnO NPs was performed by using 0.025 g of the substrate in contact with an aqueous solution of Mn(II) and Cd(II) at 500 and 550 mg/L, respectively, at 25, 30, 35 and 40 ^oC. Constant temperature shaker bath (901N0073 Fisher Scientific, U.S.A.) is used for studying the effect of wastewater temperature on the treatment process using ZnO NPs. For all experiments, the reaction mixtures were left for 24h until equilibrium followed by centrifuging at 5,000 rpm for 20 min. Then the supernatants were analyzed to measure the concentrations of Mn(II) and Cd(II) by ICP-OES (Thermo Co., model ICAP6500 Duo S.N. ICP-20101916, England) in triplicate and the mean value was reported in the analysis study. The measured repeatability in the same experiment was less than 1.0 %. The amount of Mn(II) and Cd(II) metal ions at equilibrium q_e was calculated from the mass balance equation given as below equation (**1**):

$$\mathbf{q_e = \frac{V(C_o - C_e)}{m} 100} \qquad \mathbf{(1)}$$

where q_e (mg/g) is the amount of Mn(II) or Cd(II) per mass unit of adsorbents at a certain time t. C_o and C_e (mg/L) are concentrations of Mn(II) or Cd(II) at the initial time and at time t, respectively. V is the volume of the solution (mL), and m is the mass of adsorbent (mg). The percent of metal ions removal (Adsorption %) by ZnO NPs was determined for each equilibration by the expression presented as equation (**2**):

$$\mathbf{Adsorption\ (\%) = \frac{(C_o - C_t)}{C_o} 100} \qquad \mathbf{(2)}$$

Isotherm models

The isotherm models used to describe the adsorption process in water treatment were developed by Langmuir, Freundlich and Temkin, and their constants were calculated. The Langmuir isotherm is generally used for monolayer adsorption at specific homogenous sites on adsorbents surface[40]. The Langmuir isotherm is described mathematically by equation (**3**)[41]:

$$\frac{C_e}{q_e} = \frac{1}{K_L q_m} + \frac{C_e}{q_m} \qquad \mathbf{(3)}$$

where: q_m is monolayer sorption capacity (mg/g) and K_L is Langmuir equilibrium constant (L/mg). The fundamental features of the Langmuir isotherm can be described in terms of separation factor or equilibrium parameter R_L, which is defined by the following expression equation (**4**)[42].

$$R_L = \frac{1}{1+bC_o} \quad (4)$$

The value of R_L indicates the isotherm shape to be unfavorable ($R_L > 1$), favorable ($0 < R_L < 1$) and irreversible ($R_L = 1$).

Freundlich isotherm[43] is usually used for heterogeneous surface energy systems (non-uniform distribution of sorption heat), (**Eq. 5**).

$$\log q_e = \log K_F + \frac{1}{n}\log C_e \quad (5)$$

where: K_F and n are Freundlich constants, the K_F is adsorption capacity while n is adsorption intensity; while 1/n is a function of the strength of the adsorption process.

The Temkin isotherm[42] is usually used for heterogeneous surface energy systems (non-uniform distribution of sorption heat), (**Eqs. 6&7**).

$$q_e = B \ln A + B \ln C_e \quad (6)$$

$$B = \frac{R_T}{b_T} \quad (7)$$

where A is the binding constant (L/mg) and it was related to the maximum binding energy while B is Temkin adsorption constant that is related to the sorption heat. B constant is related to sorption heat (J/mol) obtained From the Temkin plot (q_e versus ln C_e). R is the universal gas constant (8.314 J/mol K), T is the absolute temperature, 303 K.

Thermodynamic study

The changes in Gibb's free energy change, ΔG^o (kJ/mol), standard enthalpy change, ΔH^o (kJ/mol), standard entropy change, ΔS^o (kJ /mol K) of the adsorption process were calculated by using the (**Eqs. 8-10**) respectively[44].

$$\Delta G^o = -RT \ln K_d \quad (8)$$

$$K_d = C_ə / C_e \quad (9)$$

$$\ln K_d = \Delta S^o / R - \Delta H^o / RT \quad (10)$$

RESULTS AND DISCUSSION

IR spectra

The IR of ZnO NPs showed strong peaks at 608 cm^{-1} (Zn-O vibrational stretching) and the broadband at 3405 cm^{-1} for ZnO NPs corresponding to O-H has absorbed water[45&46]. The wavenumber at 1632, 1117, and 708 cm^{-1} correspond to the vibration of O-Zn-O group[47&48] (Fig. 1).

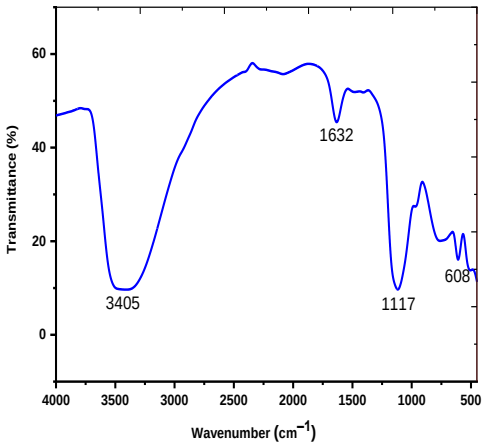

Fig. 1: FTIR spectrum of synthesized ZnO NPs

Optical study

UV-vis spectrum of the synthesized ZnO NPs was recorded in the range of 200-800 nm (Fig. 2). The spectrum of ZnO NPs is characterized by a weak absorption peak in the UV band at 268 nm that is attributed to the interband transition[49&50], whereas a broad peak around 362 nm reflects the quantum confinement of these structures[51&52].

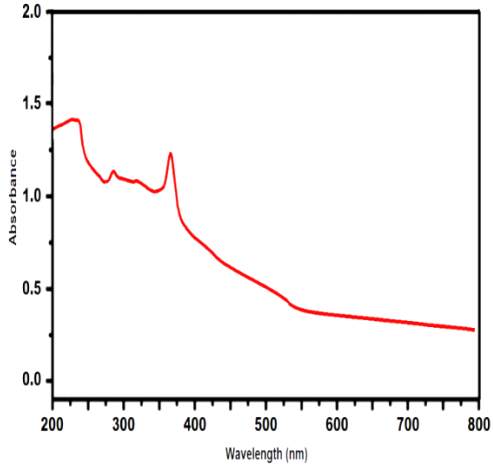

Fig. 2: UV-vis absorption spectroscopy of ZnO NPs.

UV–vis absorption provides information on the electronic structural properties of ZnO NPs sample and the shape of the absorption

peak is mainly depending on the particle size. The energy band interval is usually calculated from the relationship Tauc equation (**11**) relating the wavelength with the absorption coefficient.

$$\alpha h\nu = A\,(h\nu - E_g)^n \qquad (11)$$

where α is the optical absorption coefficient and hυ the photon energy (h is Planck's constant, ν is the frequency of light), A is a transition parameter, and E_g is the bandgap energy, n= 2 (direct) and n= ½ (indirect) transitions. The direct and indirect band gaps (Fig. 3) were obtained by extrapolating the linear region up to the energy axis by plotting $(\alpha h\upsilon)^2$ and $(\alpha h\upsilon)^{1/2}$ vs the photon energy (hυ)[53]. The as-prepared ZnO NPs has Eg wider range than the ordinary band gap which reported around 2.2-4.5 eV[54&55]. However, it is observed that the direct bandgap energy of synthesized ZnO NPs is 3.39 eV due to the quantum size effect. Similarly, the indirect bandgap energy of ZnO NPs is 1.932 eV.

PL spectroscopy was recorded for investigating the optical emission characteristic of ZnO NPs. The PL spectra of ZnO NPs excited by 325 nm excitation wavelengths are shown in (Fig. 4). Generally, there are two reasons to explain the luminescence of ZnO NPs: the structural defects in the crystals and the quantum size effect. The emission band at ~420 nm may be attributed to the surface state emission or deep trap emission which is in good agreement with a PL spectrum of nanoparticle ZnO NPs[56&57]. The emission peak at about 420 nm can be related to the combination of conduction band electrons and valence band holes. In Figure 4(B) the bandgap recorded 3.39 eV and this band gap value is an agreement with the recorded value of UV analysis (Fig. 3).

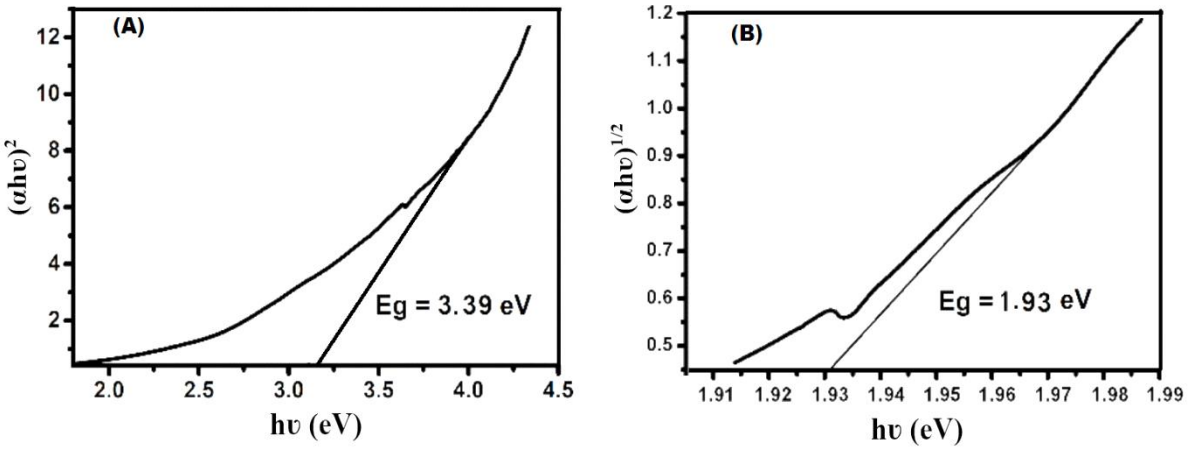

Fig. 3: Plots of $(\alpha h\upsilon)^2$ and $(\alpha h\upsilon)^{1/2}$ vs hυ (eV) for the direct and indirect bandgap ZnO NPs (A, B). The calculated direct and indirect bandgap of ZnO NPs (3.39, 1.932 eV).

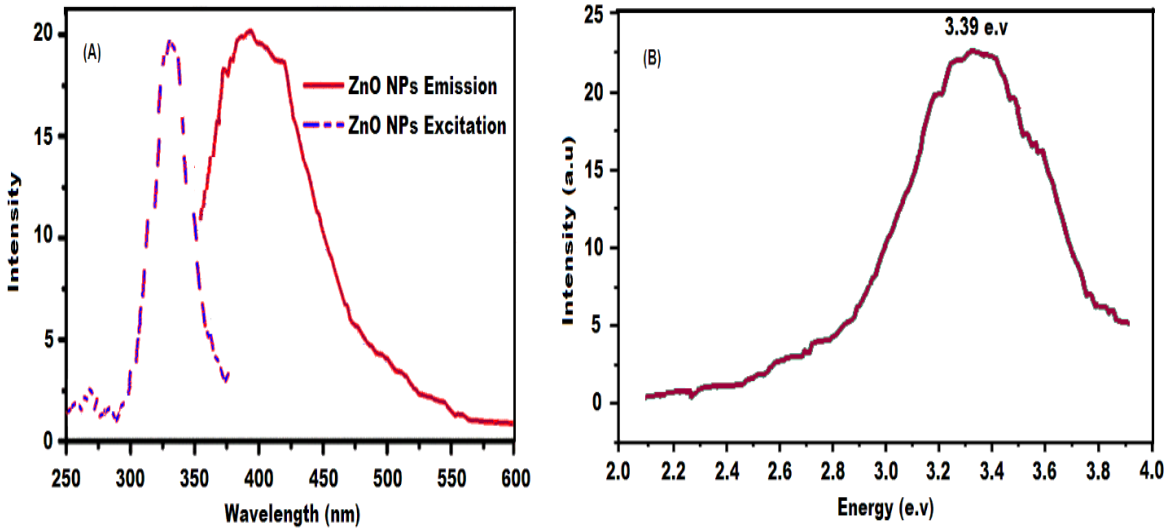

Fig. 4: Excitation and emission spectra (A), and Bandgap energy of ZnO NPs by PL spectrum (B).

SEM and TEM analysis

The morphology of the prepared adsorbent was recorded using SEM and TEM micrographs (Fig. 5). The SEM micrograph of ZnO NPs is shown in (Fig. 5(A)). The result showed that the synthesized ZnO NPs were spherical with a diameter of approximately 22.50 nm. TEM easily observed the shape and size of ZnO NPs (Fig. 5(B)). TEM image (Fig. 5(B)) show that by heating the sample, the purity of the ZnO NPs can be increased, and it is more clear. The ZnO NPs obtained showed spherical morphology with various particle diameters from 22.2 to 27.8 nm and were aggregated with numerous nanoparticles. Zang et al.[58] derived ZnO NP as hollow spheres and spheres by a solvothermal reaction in the presence of an ionic liquid (imidazolium tetrafluoroborate). The particle size distribution obtained from computed SEM and TEM images per 100 particles is presented in (Fig. 5(C&D)).

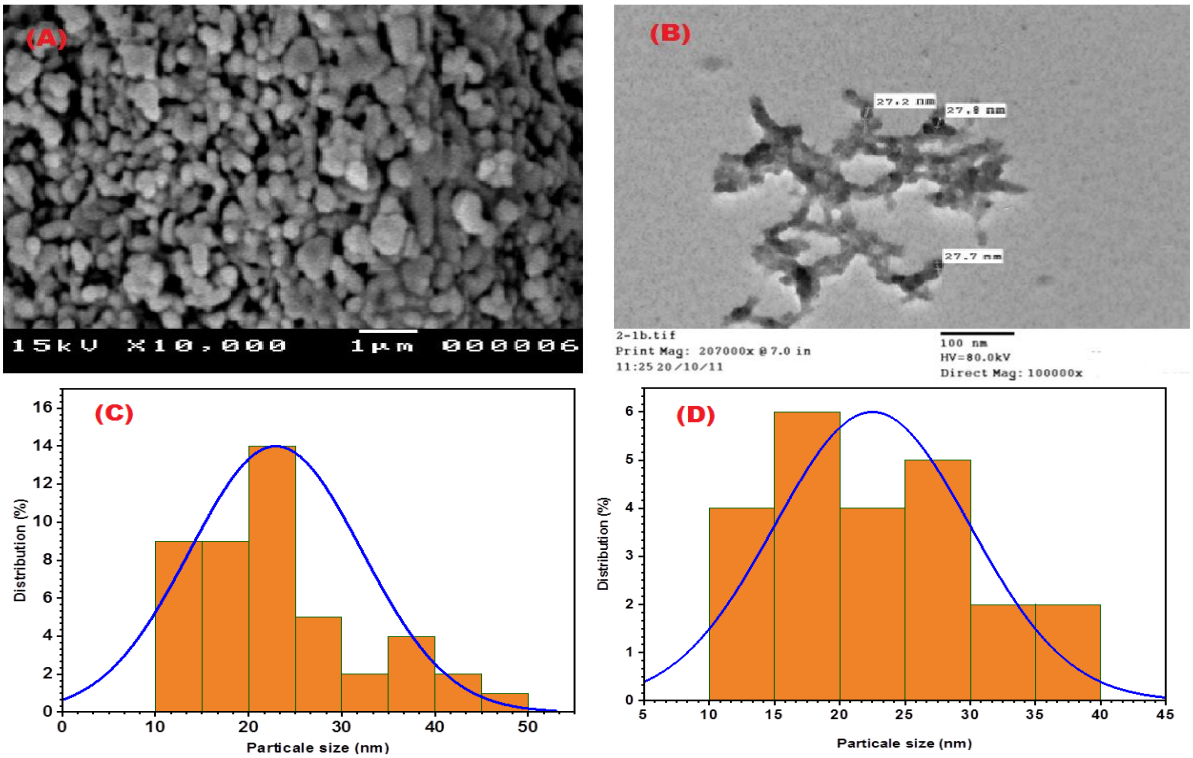

Fig. 5: SEM and TEM images of the synthesized ZnO NPs with 7.5 mL (0.1 M) of stabilizing agent, pH 11 and 60 °C; (A) SEM of ZnO NPs, (B) TEM of ZnO NPs, (C) and (D) particle size distribution for ZnO NPs.

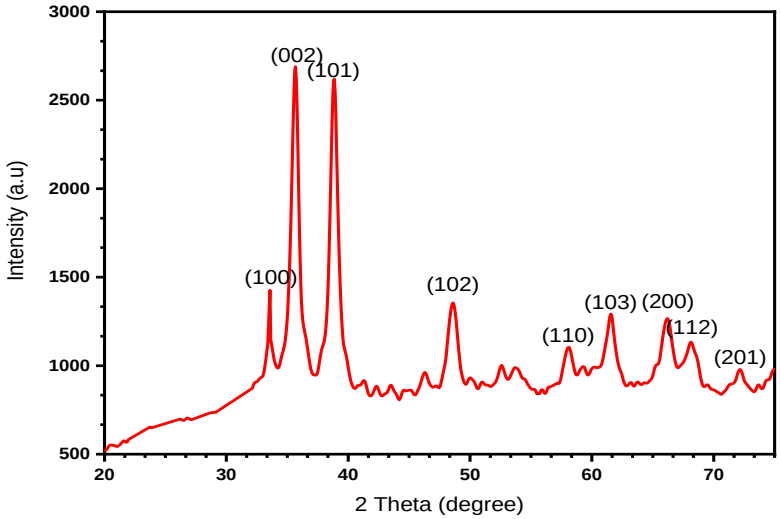

Fig. 6: XRD patterns for ZnO NPs

X-ray diffraction

The XRD models for ZnO NPs have been shown in (Fig. 6). The detected lattice peaks confirmed the presence of the ZnO NPs hexagonal phase[59&60] as depicted in JCPDS # 36-1451. The sharp intense diffraction peaks appearing at 2θ values; 32.56, 35.44, 36.58, 49.84, 57.04, 64.66, 68.26, 69.22, and 70.48 corresponding to (100), (002), (101), (102), (110), (103), (200), (112) and (201) planes of ZnO NPs with high crystallinity[61]. The instrumental broadening and the sample impact are the sources of peak breath in Bragg's effect. The full widths at half maxima "FWHM" of the measured peaks were estimated and corrected according to the Pseudo-Voigt function[62] of the line profile relation and it can be derived as the following equation (**12**):

$$\beta_{hkl} = [\beta^2_{mes.} - \beta^2_{inst.}]^{1/2} \qquad (12)$$

where β_{hkl} is the corrected FWHM, $\beta_{mes.}$ is the measured FWHM, and $\beta_{inst.}$ is the instrumental FWHM. The average crystallite size can be estimated using the Scherrer equation as the following equation (**13**):

$$D_{scher} = 0.9\lambda / \beta_{hkl} \cos(\theta_{hkl}) \qquad (13)$$

where, D= Average crystallite size, λ= 1.54056 Å, β is a full width in radians at half maximum of the peak (in radians), θ= Bragg's angle. The average grain sizes were determined from the XRD powder pattern according to Debey-Scherrer's equation (**14**):

$$D = k\lambda / \beta \cos\theta \qquad (14)$$

where D is the average grain size, k is a constant equal to 0.89, λ is the wavelength of x-rays equal to 0.1542 nm and β is the full width of diffraction peak under consideration (rad) in the middle of its height that was considered after computer-fit of the x-ray data using the *Gaussian* line shape, and θ is Bragg's angle. Tables 2 shows the average crystallite sizes for the ZnO NPs computed by the XRD line broadening method[63]. The calculated mean particle size for the ZnO NPs sample from XRD, SEM and TEM micrographs is tabulated in Table 3. The values of zinc nanoparticles calculated by different methods in the Table 3 indicate the high purity of the prepared ZnO NPs.

Table 2: XRD characteristics and the estimated structural parameters of ZnO NPs (λ = 0.1541838 nm)

Parameters	Plane								
Miller indices	(100)	(002)	(101)	(102)	(110)	(103)	(200)	(112)	(101)
$h^2 + k^2 + l^2$	1	4	2	5	2	7	4	9	2
$2\theta_{mesured}$	32.56	35.44	36.58	49.84	57.04	64.66	68.26	69.22	72.48
$\theta_{mesured}$ in degree	16.28	17.72	18.29	24.92	28.52	32.33	34.13	34.61	36.24
$\theta_{mesured}$ in radian	0.284	0.309	0.319	0.434	0.497	0.564	0.595	0.604	0.632
Gaussian $FWHM_{mesured}$ from origin ($\beta_{mesured}$) in degree	0.36	0.48	0.42	0.90	0.48	0.48	0.42	0.66	0.60
Gaussian $FWHM_{mesured}$ from origin ($\beta_{mesured}$) in radian	0.005	0.008	0.007	0.016	0.008	0.008	0.007	0.012	0.010
$FWHM_{instrument}$ ($\beta_{instrument}$) in degree	0.16								
$FWHM_{instrument}$ ($\beta_{instrument}$) in radian	0.003								
Gaussian β_d = sqrt ($\beta^2_{mesured}$- $\beta^2_{instrument}$) in radian	0.006	0.007	0.006	0.015	0.007	0.008	0.007	0.010	0.010
Gaussian ($1/\beta_d$)	177.7	126.6	147.5	64.7	126.6	126.6	147.5	89.5	99.0
$Sin\theta_{mesured}$	0.280	0.304	0.314	0.421	0.477	0.535	0.561	0.567	0.591
$Sin^2\theta_{mesured}$	0.078	0.092	0.098	0.178	0.228	0.286	0.315	0.322	0.349
Placing distance (d) = λ/2 sin θ	0.047	0.044	0.042	0.031	0.027	0.024	0.023	0.021	0.021
$Cos\ \theta_{mesured}$	0.956	0.952	0.949	0.907	0.878	0.845	0.828	0.823	0.806
Gaussian β_d $Cos\ \theta_{mesured}$	0.346	0.457	0.399	0.816	0.422	0.405	0.348	0.543	0.483
$Cos^2\ \theta_{mesured}$	0.921	0.907	0.902	0.822	0.772	0.714	0.685	0.677	0.650
$Tan\ \theta_{mesured}$	0.292	0.319	0.331	0.465	0.543	0.633	0.678	0.690	0.732
Gaussian $D_{scher} = 0.9\lambda/ \beta_d \cos\theta_{mesured}$ in nm	35.68	28.44	26.56	9.90	20.00	20.79	24.73	15.09	17.05
Lattice constants (a) $a = d\ h^2+k^2+l^2$ in Å	0.047	0.176	0.084	0.155	0.054	0.168	0.092	0.189	0.042
Gaussian average D_{scher} in nm	19.71								

Table 3. The calculated average crystallite size of ZnO NPs.

Sample	The average crystallite size (nm)		
	XRD method	SEM (SD)	TEM (SD)
ZnO NPs	19.71	22.92 (9.23)	22.50 (7.48)

Adsorption process

All desorption tests of Mn(II) and Cd((II) ions removal by nano-adsorbent, ZnO NPs from aqueous solutions, were carried out using a batch method. The process of removing Mn(II) and Cd(II) ions from wastewater such as contact time, the concentration of hydrogen ion concentrations (pH), amount of adsorbent, and the temperature of solutions, all these factors are studied.

Effect of contact time

The effect of contact time on Mn(II) and Cd(II) ions sorption was studied in different time intervals ranging from 0 min to 180 min with the initial metal concentration of Mn(II) is 500 mg/L and Cd(II) is 550 mg/L and at pH= 7 and 0.25 g (ZnO NPs) and 350 rpm agitation. (Fig. 7) illustrates the sorption of Mn(II) and Cd(II) ions by ZnO NPs with respect to contact time. At 0-90 min, absorption of Mn(II) and Cd(II) ions was increased sharply. Afterward, the percent removal was remained steady and, in some cases, decreased at higher times. This can be attributed to the desorption of Mn(II) and Cd(II) ions from the surface of the nanoadsorbent for a long time of contact with the aqueous medium. This shows that ZnO NP material is more selective. The best uptake rate of ZnO NP can be attributed to its high specific surface area. Since there is no significant increase in sorption Mn(II) and Cd(II) when the time is 100 min., the equilibration time could be considered to be 180 minutes, to ensure complete sorption. The slight increase in the percentage removal of heavy metal ions from the aqueous solution was observed by ZnO NPs, 91 % and 93 % for Mn(II) and Cd(II), respectively. The percentage removal of Mn(II) and Cd(II) increases with increasing time.

Effect of Dosage

For studying the effect of dosage we take a different amount of ZnO NPs adsorbent (from 0 to 2 gm) at pH= 7 and 350 rpm agitation for 2hrs. after that we measured Mn(II) and Cd(II) concentrations. Initially, the rate of adsorption was very rapid up to 0.25 g/L for ZnO NPs. This is because, at a higher dose of adsorbent, more adsorption sites are available, leading to greater elimination of Mn(II) and Cd(II) ions. Above 0.50 g/L removal of metal ions becomes very slow, as the surface of Mn(II) and Cd(II) ions and the solution concentration come to equilibrium with each other. The adsorbant dose of 0.25 g/L was therefore used in all subsequent experiments. The relationship between the amount of ZnO NPs and the amount of heavy metal adsorption is presented in (Fig. 8). The % removal of heavy metal ions from the aqueous solution was observed by ZnO NPs, 72 % and 77 % for Mn(II) and Cd(II), respectively.

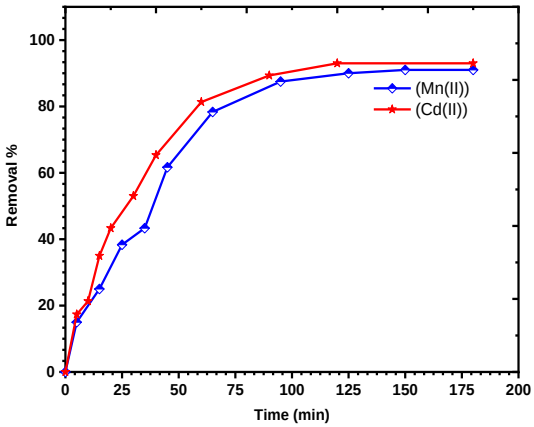

Fig. 7: Effect of contact time on Mn(II) and Cd(II) adsorptions by ZnO NPs adsorbent; (500 and 550 mg/L initial Mn(II) and Cd(II) concentrations, respectively with 0.25 g adsorbent dose, temperature 30 ^{o}C and pH = 7).

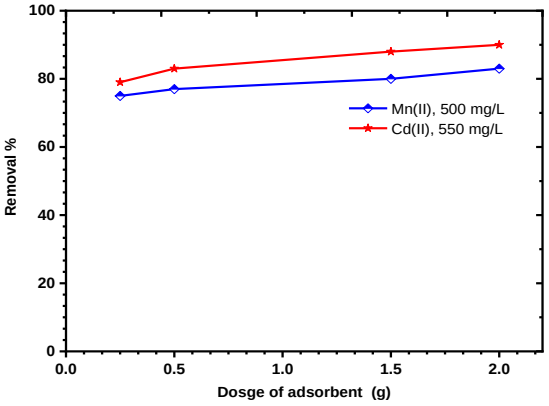

Fig. 8: Effect of adsorbent dosage on removal of Mn(II) and Cd(II) ions, adsorbent dose up to 2 g, 350 rpm agitation, and pH = 7.

Effect of pH

(Fig. 9) demonstrates pH-based adsorption capacity for Mn(II) and Cd(II) ions, for 24 hrs. contact time at 500 and 550 mg/L as an initial Mn(II) and Cd(II) concentrations and solid/liquid ratio of 1 g/L. The removal of Mn(II) and Cd(II) from water by prepared adsorbent ZnO NPs was found to be highly dependent on the solution pH value, which affects the surface charge of the adsorbent and degree of ionization and speciation of the adsorbent[64]. The highest adsorption capacity was noted of the ZnO NPs for Cd(II) ion. As the pH of the sorption solution increased the interaction with Mn(II) and Cd(II) ions is favorable, leading to enhance the adsorption capacity until Mn(II) and Cd(II) ions tend to hydrolyze. After pH= 6.0, the adsorption capacity increases remarkably[65]. The implications of Mn(II) and Cd(II) hydrolysis at higher solution pH are: (i) due to a lower residual charge, $Mn(OH)^+$ and $Cd(OH)^+$ species have less affinity to the ZnO NPs surface compared to Mn(II) and Cd(II) ions; and (ii) at higher pH values, precipitation of $Mn(OH)_2$ and $Cd(OH)_2$ or electrostatic repulsion of negative species by ZnO NPs (the negatively charged surface) can prevent the uptake of Mn(II) and Cd(II) ions[66].

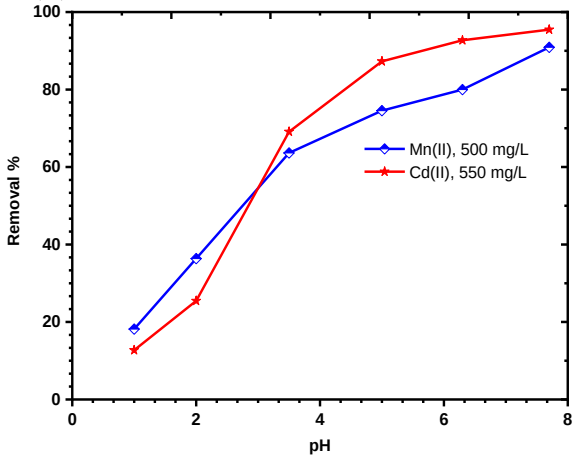

Fig. 9: Effect of pH on adsorption of Mn(II) and Cd(II) by ZnO NPs adsorbent, (500 mg/L and 550 mg/L initial Mn(II) and Cd(II) concentrations respectively, 0.25 g adsorbent dose, temperature 30 ^oC, 24 hrs.).

The results showed that the removal of Mn(II) andCd(II) ions increased significantly as the pH increased up to 7. It was noticed that when the pH value is higher than 5, the adsorption amount increased dramatically, which was attributed to the fact that heavy metal ions started to precipitate leading to the reduction of the metal ions in the aqueous solution at higher pH value, pH increases may change the phase structure and the stoichiometry of the forming phases.

Adsorption isotherms

Experimental isotherms are important for the description of sorption capacity to help assess the feasibility of the process for a given adsorbent. The isotherm plays a critical role in the predictive modeling procedures for the design of sorption systems and analysis. Among these models, the most used to describe the adsorption process in water treatment were developed by Langmuir, Freundlich, and Temkin. Experimental and calculated data were listed.

Langmuir isotherm

In this study, the plot of C_e/q_e versus C_e yields a straight line shown in (Fig. 10), and calculated values are listed in Table 4. The results revealed that the adsorption process suited well to the Langmuir model with R^2 values of 0.9998, 0.9998, and 0.9981 for ZnO NPs. Better fitted Langmuir isotherm model suggested the homogenous adsorption of Mn(II) and Cd(II) cations with the adsorption active site of equal affinity. The separation factor, R_L, values determined from the Langmuir model for Mn(II) and Cd(II) removal were in the range of 0.031-0.018 suggesting that the removal of Mn(II) and Cd(II) was favorable.

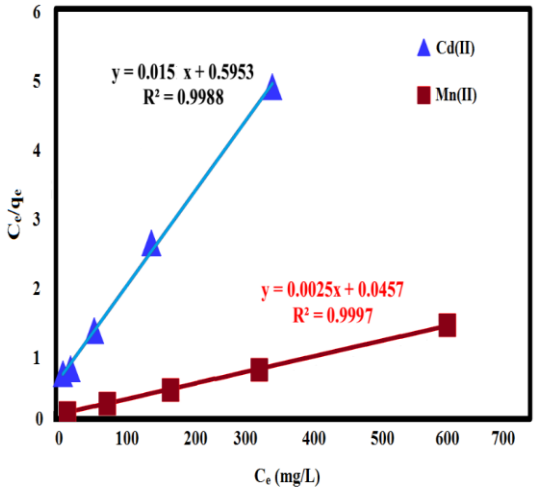

Fig. 10: Plot of C_e/q_e versus C_e for estimation of the correlation coefficient, R^2, of the Langmuir model.

Freundlich isotherm

The Freundlich isotherm is usually used for heterogeneous surface energy systems (non-uniform distribution of sorption heat). The log q_e vs log C_e plot allows determining the Freundlich constants. The results of Freundlich adsorption isotherm models are shown in (Fig. 11). The adsorption constants and the correlation coefficients are also listed in Table 4. If a value of 1/n is below one, it indicates a normal adsorption process. On the other hand, 1/n being above one indicates the cooperative adsorption process. In this study the 1/n values lie between 0 and 1; this indicates a normal adsorption process of Mn(II) and Cd(II) adsorption onto ZnO NPs adsorbent. Also, n value lies between one and ten; this indicates a favorable adsorption process. As given in Table 4, the values of R^2 have been recorded 0.9877, and 0.9656 for ZnO NPs adsorbent of Mn(II) and Cd(II) respectively. This indicates that the Freundlich isotherm was not the best fit for the sorption process of Mn(II) and Cd(II) onto the surface of the adsorbent. Therefore, the removal of Mn(II) and Cd(II) ions onto ZnO NPs surface proceed with some heterogeneity inactive sites.

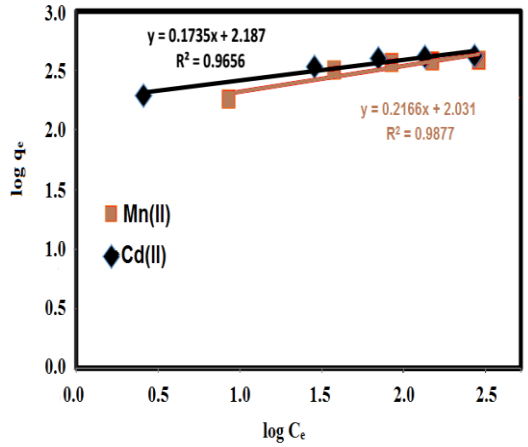

Fig. 11: The plot of log q_e versus log C_e for estimation of correlation coefficient; R^2 of the Freundlich model.

Temkin isotherm

Temkin model which assumed that the adsorption heat would decrease by increasing the adsorbent mass was also used to analyze adsorption data, shown in (Fig. 12). According to calculated Temkin parameters A and B, Table 4, values were found to be 1.77 L/g, 59.90 J/mol, 10.40 L/g and 51.07 J/mol, in the case of ZnO NPs for Mn(II) and Cd(II) respectively, indicating that the heat of sorption refers to a physical process. Due to a weak interaction between Mn(II) and Cd(II) ions and prepared ZnO NPs surfaces[42]. Furthermore, the b_T values recorded 0.042, and 0.048 KJ/mol for Mn(II) and Cd(II) onto ZnO NPs adsorbent, respectively, which confirmed that the removal occurred through physisorption process[67].

Comparing R^2 values in Table 4, it is found that the highest values were recorded for the Langmuir isotherm model. Therefore, Langmuir isotherm was the best fitted in sorption. The adsorption isotherms are followed in an order: Langmuir > Freundlich > Temkin.

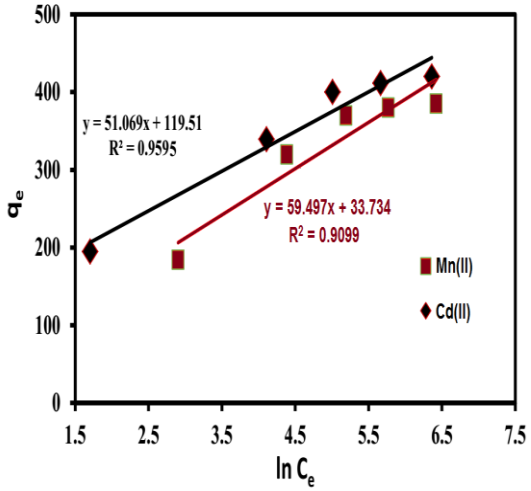

Fig. 12: The plot of ln q_e versus ln C_e for estimation of correlation coefficient; R^2; of Temkin model.

Adsorption performance evaluation

A comparison of the sorption performance of prepared nano-adsorbent with other reported adsorbents for some cations was shown in Table 5. In the Table 5 are some nanomaterials prepared by different methods. Moreover, it has a high cost compared to the ZnO NPs under study, which can be prepared in more quantities with less cost. The synthesized ZnO NPs is considered to has the outstanding capability to adsorb Mn(II) and Cd(II) cations compared to various nano-adsorbents to remove other cations from aqueous solution (Table 5). The adsorption capacity of ZnO NPs for both Mn(II) and Cd(II) cations were 391.6 and 437.2 mg/g. The excellent adsorption capacity of the synthesized nanomaterial, in this study, was attributed to the high specific surface area and dispersion of ZnO NPs sample.

Table 4: Isotherm parameters for Mn(II) and Cd(II) removal onto ZnO NPs

Cations	Isotherm models		
	Langmuir	Freundlich	Temkin
Mn(II)	q_m = 397 K_L = 0.054 R_L = 0.031 R^2 = 0.9997	K_F = 107 n = 4.6 R^2 = 0.9877	A = 1.77 B = 59.9 b_T = 0.042 R^2 = 0.9659
Cd(II)	q_m = 427 K_L = 0.091 R_L = 0.018 R^2 = 0.9988	K_F = 152 n = 5.7 R^2 = 0.9656	A = 10.40 B = 51.07 b_T = 0.048 R^2 = 0.9859

Table 5: Different nanocomposites-based metal oxides used as adsorbents for metal ions removal from aqueous solution

Nanomaterials	Adsorption capacity (mg/g)	Analyte
TiO2/graphene oxide[85]	72.8 65.6	Cd(II) Pb(II)
Fe_3O_4/chitosan/graphene oxide[86]	76.9	Pb(II)
Phosphonium-coated MNPs[87]	50.5 32.2	As(V) Cr(VI)
SiO_2/graphene[88]	113.6	Pb(II)
Fe-Mn binary oxide-biochar[89]	95.2	Cd(II)
Co–Al–Fe[90]	130 76	As(III) As(V)
ZnO NPs (Current study)	391.6 437.2	Mn(II) Cd(II)

Thermodynamics study

To investigate the sorption process of Mn(II) and Cd(II) in-depth, the typical thermodynamic parameters are determined. The calculated thermodynamic parameters, Figure 13, are listed in Table 6. In general, the value of $\Delta H^o < 0$ indicated that the sorption process was an exothermic reaction. As the temperature increased the value of ΔG° increased. The positive value of ΔG° under various temperatures denoted that the reaction was a nonspontaneous process[74]. From Table 6, the ΔG° value of ZnO NPs adsorbent are negative indicating the two reactions are a spontaneous and thermodynamically feasible process. As illustrated in (Fig. 13), a higher temperature enhances the adsorption reaction, and the values of ΔH^o are positive. In a work, Ren et al.[75] noticed that the adsorption capacity of the graphene/MnO_2 composite increased from 46 to 60 mg/g when the reaction temperature from 298 K to 318 K. In this study, at 313 K the adsorption capacity of ZnO NPs nanoparticle is observed to be 1.2 times higher than for those recorded at 298 K. The ΔS^o of two adsorbents are positive, indicating that the randomness at the adsorbent / Mn(II) or Cd(II) solution interface increased as the process progressed[76&77]. The values of ΔH^o were ranged from 37 to 41 kJ/mol, illustrating that physisorption existed for the adsorption of Mn(II) and Cd(II) on the prepared adsorbent.

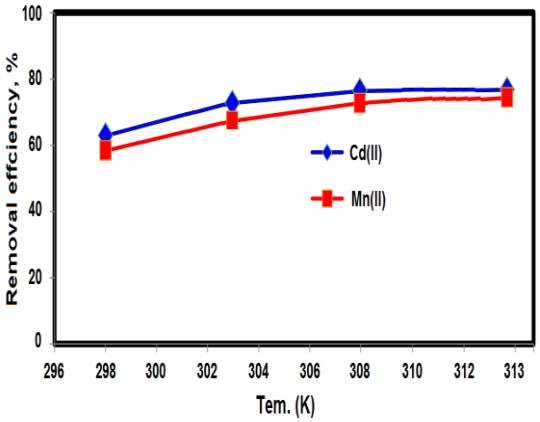

Fig. 13: Effect of temperature (K) in adsorption of Mn(II) and Cd(II) by ZnO NPs adsorbent. (500, 550 mg/L initial Mn(II) and Cd(II) concentration respectively, 0.25 g adsorbent dose, temperature 30 ^oC, 24hrs.).

Table 6: Thermodynamic parameters for Mn(II) and Cd(II) adsorption by ZnO NPs as adsorbent.

Ions	Temperature (K)	K_d (L/mg)	ΔG^o (kJ/mol)	ΔH^o (kJ/mol)	ΔS^o (J /mol. K)
Mn(II)	298	1.41	-1.00	41.98	144.88
	303	2.06	-1.81		
	308	2.67	-2.51		
	313	2.93	-2.73		
Cd(II)	298	1.83	-1.47	37.58	131.90
	303	2.66	-2.45		
	308	3.21	-2.97		
	313	3.28	-3.08		

Conclusion

In this study, the preparation and characterization of ZnO NPs have been investigated. Parameters of the precipitation conditions like pH, component ratio, and aging temperature have been studied in detail. Precipitates obtained from different conditions were characterized by several techniques like UV-visible spectrophotometer, photoluminescence spectroscopy, SEM, TEM, XRD, and FT-IR. ZnO NPs showed an absorption peak at 362 nm with a wide direct bandgap (3.39 eV). PL spectra showed the emission peak at 420 and 325 nm excitation wavelengths for ZnO NPs. The average crystallite sizes for the ZnO NPs nanoparticle were calculated by the XRD line broadening method and confirmed with TEM and SEM micrographs summations. The calculated average crystallite sizes of ZnO NPs were with average lengths of 19.71 nm. TEM observations showed that the as-produced ZnO NPs is spherical with different diameters in the range 22.2–27.8 nm. Furthermore, the produced nanomaterial show exceptional adsorption capability for Mn(II) and Cd(II) removal from water, the adsorption capacities were found to be 391.6 and 437.2 mg/g for Mn(II) and Cd(II) respectively. The adsorption isotherms could be well described by the Langmuir, Freundlich, and Temkin isotherm models. Thermodynamically, the adsorption processes were spontaneous, endothermic, and physical in nature, for ZnO NPs. The high removal efficiency of Mn(II) and Cd(II) by ZnO NPs with its exceptional adsorption capability suggests that the ZnO NPs has great potential applications in environmental protection.

REFERENCES

1- F. D. Auret, S. A. Goodman, M. Hayes, M. J. Legodi, H. A. Van Laarhoven and D. C. Look, ″The influence of high energy proton bombardment on the electrical and defect properties of single-crystal ZnO″, ***Journal of Physics: Condensed Matter***, 13 (40), 8789-8792 (2001).

2- A. Kołodziejczak-Radzimska and T. Jesionowski, ″Zinc oxide-from synthesis to application: a review″, ***Materials***, 7 (4), 2833-2881 (2014).

3- G. P. Barreto, G. Morales and M. L. L. Quintanilla, ″Microwave assisted synthesis of ZnO nanoparticles: effect of precursor reagents, temperature, irradiation time, and additives on nano-ZnO morphology development″, ***Journal of Materials***, *2013*, 1-11(2013).

4- P. Banerjee, S. Chakrabarti, S. Maitra and B. K. Dutta, ″Zinc oxide nano-particles–sonochemical synthesis, characterization and application for photo-remediation of heavy metal″, ***Ultrasonics Sonochemistry***, 19 (1), 85-93 (2012).

5- M. Khatami, H. Q. Alijani, H. Heli and I. Sharifi, ″Rectangular shaped zinc oxide nanoparticles: Green synthesis by Stevia and its biomedical

efficiency″, ***Ceramics International***, 44 (13), 15596-15602 (2018).
6- J. Wojnarowicz, T. Chudoba and W. Lojkowski, ″A review of microwave synthesis of zinc oxide nanomaterials: Reactants, process parameters and morphologies″, ***Nanomaterials***, 10 (6), 1086-1226 (2020).
7- A. Sirelkhatim, S. Mahmud, A. Seeni, N. H. M. Kaus, L. C. Ann, S. K. M. Bakhori and D. Mohamad, ″Review on zinc oxide nanoparticles: antibacterial activity and toxicity mechanism″, ***Nano-micro Letters***, 7 (3), 219-242 (2015).
8- A. Abdolhoseinzadeh and S. Sheibani, ″Enhanced photocatalytic performance of Cu_2O nano-photocatalyst powder modified by ball milling and ZnO″, ***Advanced Powder Technology***, 31 (1), 40-50 (2020).
9- F. J. Heiligtag and M. Niederberger, ″The fascinating world of nanoparticle research″, ***Materials Today***, 16 (7-8), 262-271 (2013).
10- Y. B. Hahn, ″Zinc oxide nanostructures and their applications″, ***Korean Journal of Chemical Engineering***, 28 (9), 1797-1813 (2011).
11- T. Frade, M. M. Jorge and A. Gomes, ″One-dimensional ZnO nanostructured films: Effect of oxide nanoparticles″, ***Materials Letters***, 82, 13-15 (2012).
12- Wahab, R., Ansari, S. G., Kim, Y. S., Seo, H. K., & Shin, H. S. (2007). Room temperature synthesis of needle-shaped ZnO nanorods via sonochemical method. ***Applied Surface Science***, *253*(18), 7622-7626.
13- X. Y. Kong, Y. Ding, R. Yang and Z. L. Wang, ″Single-crystal nanorings formed by epitaxial self-coiling of polar nanobelts″, ***Science***, 303 (5662), 1348-1351 (2004).
14- Z. W. Pan and Z. L. Wang, ″Nanobelts of semiconducting oxides″, ***Science***, *291* (5510), 1947-1949 (2001).
15- W. J. Chen, W. L. Liu, S. H. Hsieh and T. K. Tsai, ″Preparation of nanosized ZnO using α brass″, ***Applied Surface Science***, 253 (16), 6749-6753 (2007).
16- J. Liu, X. Huang, J. Duan, H. Ai and P. Tu, ″A low-temperature synthesis of multiwhisker-based zinc oxide micron crystals″, ***Materials Letters***, 59 (28), 3710-3714 (2005).
17- Y. Huang, J. He, Y. Zhang, Y. Dai, Y. Gu, S. Wang and C. Zhou, ″Morphology, structures and properties of ZnO nanobelts fabricated by Zn-powder evaporation without catalyst at lower temperature″, ***Journal of Materials Science***, *41* (10), 3057-3062 (2006).
18- B. Nikoobakht, X. Wang, A. Herzing and J. Shi, ″Scalable synthesis and device integration of self-registered one-dimensional zinc oxide nanostructures and related materials″, ***Chemical Society Reviews***, *42*(1), 342-365 (2013).
19- W. S. Chiu, P. S. Khiew, M. Cloke, D. Isa, T. K. Tan, S. Radiman and C. H. Chia, ″Photocatalytic study of two-dimensional ZnO nanopellets in the decomposition of methylene blue″, ***Chemical Engineering Journal***, *158* (2), 345-352 (2010).
20- M. Jose-Yacaman, C. Gutierrez-Wing, M. Miki, D. Q. Yang, K. N. Piyakis and E. Sacher, ″Surface diffusion and coalescence of mobile metal nanoparticles″, ***The Journal of Physical Chemistry B***, *109* (19), 9703-9711 (2005).
21- M. F. Al-Hakkani, G. A. Gouda and S. H. Hassan, ″A review of green methods for phyto-fabrication of hematite (α-Fe_2O_3) nanoparticles and their characterization, properties, and applications″, ***Heliyon***, 7 (1), e05806 (2021).

22- M. S. Saddik, F. M. Alsharif, M. A. El-Mokhtar, M. F. Al-Hakkani, M. M. El-Mahdy, H. S. Farghaly and H. A. Abou-Taleb, ″Biosynthesis, characterization, and wound-healing activity of phenytoin-loaded copper nanoparticles″, ***AAPS PharmSciTech***, 21 (5), 1-12 (2020).
23- H. M. Yusof, R. Mohamad and U. H. Zaidan, ″Microbial synthesis of zinc oxide nanoparticles and their potential application as an antimicrobial agent and a feed supplement in animal industry: a review″, ***Journal of Animal Science and Biotechnology***, 10 (1), 1-22 (2019).
24- N. M. Shamhari, B. S. Wee, S. F. Chin and K. Y. Kok, ″Synthesis and characterization of zinc oxide nanoparticles with small particle size distribution″, ***Acta Chimica Slovenica***, 65(3), 578-585 (2018).
25- S. Alamdari, M. S. Ghamsari, C. Lee, W. Han, H. H. Park, M. J. Tafreshi and M. H. M. Ara, ″Preparation and characterization of zinc oxide nanoparticles using leaf extract of Sambucus ebulus″, ***Applied Sciences***, 10 (10), 3620 (2020).
26- S. Alamdari, M. S. Ghamsari and M. J. Tafreshi, ″Optimization of Gallium concentration to improve the performance of ZnO nanopowders for nanophotonic applications″, ***Ceramics International***, 46 (4), 4484-4492 (2020).
27- A. Raja, S. Ashokkumar, R. P. Marthandam, J. Jayachandiran, C. P. Khatiwada, K. Kaviyarasu, R.G. Raman and M. Swaminathan, ″Eco-friendly preparation of zinc oxide nanoparticles using Tabernaemontana divaricata and its photocatalytic and antimicrobial activity″, ***Journal of Photochemistry and Photobiology B: Biology***, 181, 53-58 (2018).
28- K. Steffy, G. Shanthi, A. S. Maroky and S. Selvakumar, ″Enhanced antibacterial effects of green synthesized ZnO NPs using Aristolochia indica against Multi-drug resistant bacterial pathogens from Diabetic Foot Ulcer″, ***Journal of Infection and Public Health***, 11 (4), 463-471 (2018).
29- J. H. Duffus, ″“Heavy metals” a meaningless term. (IUPAC Technical Report)″, ***Pure and Applied Chemistry***, 74(5), 793-807 (2002).
30- G. Pandey and S. Madhuri, ″Heavy metals causing toxicity in animals and fishes″, ***Research Journal of Animal, Veterinary and Fishery Sciences***, 2 (2), 17-23 (2014).
31- H. Cheng, Y. Hu, J. Luo, B. Xu and J. Zhao, ″Geochemical processes controlling fate and transport of arsenic in acid mine drainage (AMD) and natural systems″, ***Journal of hazardous materials***, 165 (1-3), 13-26 (2009).
32- N. J. Raju, ″Arsenic in the geo-environment: A review of sources, geochemical processes, toxicity and removal technologies″, ***Environmental Research***, 111782 (2021).
33- W. S. Wan Ngah and K. H. Liang, ″Adsorption of gold (III) ions onto chitosan and N-carboxymethyl chitosan: equilibrium studies″, ***Industrial & Engineering Chemistry Research***, 38(4), 1411-1414 (1999).
34- M. M. Reglero, M. A. Taggart, L. Monsalve-Gonzalez and R. Mateo, ″Heavy metal exposure in large game from a lead mining area: effects on oxidative stress and fatty acid composition in liver″, ***Environmental Pollution***, 157 (4), 1388-1395 (2009).
35- A. A. Gybina and J. R. Prohaska, ″Copper deficiency results in AMP-activated protein kinase activation and acetylCoA carboxylase phosphorylation in rat cerebellum″, ***Brain Research***, 1204, 69-76 (2008).
36- M. Cheraghi, B. Lorestani and N. Yousefi, ″Effect of wastewater on heavy metal accumulation in Hamedan Province vegetables″,

International Journal of Botany, 5 (2), 109-193 (2009).

37- T. Vincent and E. Guibal, ″Chitosan-supported palladium catalyst. 5. Nitrophenol degradation using palladium supported on hollow chitosan fibers″, ***Environmental Science & Technology***, 38 (15), 4233-4240 (2004).

38- L. Zhang and Y. J. Zhu, ″ZnO micro- and nano-structures: microwave-assisted solvothermal synthesis, morphology control and photocatalytic properties″, ***Applied Physics A***, 97 (4), 847-852 (2009).

39- M. Q. Sadr, N. Assi, S. Pourmand, M. Darwish and A. Pakzad, ″Photocatalytic activity of ZnO nanoparticles prepared by a microwave method in ethylene glycol and polyethylene glycol media: A comparative study″, ***In Journal of Nano Research, Trans Tech Publications Ltd.***, 42, 53-64 (2016).

40- N. Atar, A. Olgun and S. Wang, ″Adsorption of cadmium (II) and zinc (II) on boron enrichment process waste in aqueous solutions: Batch and fixed-bed system studies″, ***Chemical Engineering Journal***, 192, 1-7 (2012).

41- M. Erhayem, F. Al-Tohami, R. Mohamed and K. Ahmida, ″Isotherm, kinetic and thermodynamic studies for the sorption of mercury (II) onto activated carbon from Rosmarinus officinalis leaves″, ***American Journal of Analytical Chemistry***, 6 (01), 1-10 (2015).

42- A. Dada, A. Olalekan, A. Olatunya and O. Dada, ″Langmuir, Freundlich, Temkin and Dubinin-Radushkevich isotherms studies of equilibrium sorption of Zn^{2+} unto phosphoric acid modified rice husk″, ***IOSR Journal of Applied Chemistry***, 3 (1), 38-45 (2012).

43- N. A. El Essawy, S. M. Ali, H. A. Farag, A. H. Konsowa, M. Elnouby and H. A. Hamad, ″Green synthesis of graphene from recycled PET bottle wastes for use in the adsorption of dyes in aqueous solution″, ***Ecotoxicology and Environmental Safety***, 145, 57-68 (2017).

44- K. B. Fontana, E. S. Chaves, J. D. Sanchez, E. R. Watanabe, J. M. Pietrobelli and G. G. Lenzi, ″Textile dye removal from aqueous solutions by malt bagasse: isotherm, kinetic and thermodynamic studies″, ***Ecotoxicology and Environmental Safety***, 124, 329-336 (2016).

45- M. Stan, A. Popa, D. Toloman, T. D. Silipas and D. C. Vodnar, ″Antibacterial and antioxidant activities of ZnO nanoparticles synthesized using extracts of Allium sativum, Rosmarinus officinalis and Ocimum basilicum″, ***Acta Metallurgica Sinica (English Letters)***, 29 (3), 228-236 (2016).

46- M. Vafaee and M. S. Ghamsari, ″Preparation and characterization of ZnO nanoparticles by a novel sol-gel route″, ***Materials Letters***, 61 (14-15), 3265-3268 (2007).

47- A. A. Aly, A. H. Osman, M. A. El-Mottaleb and G. A. Gouda, ″Reactivity of certain biologically important Azoles and morpholine towards Ni (II) and Cu (II) complexes of o-hydroxyacetophenoneethanolimine and N-Salicylidene derivatives″, ***Bulletin of Pharmaceutical Sciences. Assiut***, 29 (1), 134-149 (2006).

48- R. Al-Gaashani, S. Radiman, A. R. Daud, N. Tabet and Y. J. C. I. Al-Douri, ″XPS and optical studies of different morphologies of ZnO nanostructures prepared by microwave methods″, ***Ceramics International***, 39 (3), 2283-2292 (2013).

49- N. S. Pesika, K. J. Stebe and P. C. Searson, ″Determination of the

particle size distribution of quantum nanocrystals from absorbance spectra", ***Advanced Materials***, 15 (15), 1289-1291 (2003).
50- K. Karthik, S. Dhanuskodi, C. Gobinath, S. Prabukumar and S. Sivaramakrishnan, "Nanostructured CdO–NiO composite for multifunctional applications", ***Journal of Physics and Chemistry of Solids***, 112, 106-118 (2018).
51- G. S. Dhillon, S. Kaur and S. K. Brar, "Facile fabrication and characterization of chitosan-based zinc oxide nanoparticles and evaluation of their antimicrobial and antibiofilm activity", ***International Nano Letters***, 4 (2), 107 (2014).
52- S. Alamdari, M. S. Ghamsari, C. Lee, W. Han, H. H. Park, M. J. Tafreshi and M. H. M. Ara, "Preparation and characterization of zinc oxide nanoparticles using leaf extract of Sambucus ebulus", ***Applied Sciences***, 10 (10), 3620 (2020).
53- A. M. Mostafa, S. A. Yousef, W. H. Eisa, M. A. Ewaida and E. A. Al-Ashkar, "Synthesis of cadmium oxide nanoparticles by pulsed laser ablation in liquid environment", ***Optik***, 144, 679-684 (2017).
54- Z. Y. Zhang and H. M. Xiong, "Photoluminescent ZnO nanoparticles and their biological applications", ***Materials***, 8 (6), 3101-3127 (2015).
55- P. Camarda, R. Schneider, R. Popescu, L. Vaccaro, F. Messina, G. Buscarino and M. Cannas, "Effect of thermal annealing on the luminescence of defective ZnO nanoparticles synthesized by pulsed laser ablation in water", ***Physica Status Solidi (C)***, 13 (10-12), 890-894 (2016).
56- X. Wang, Y. Ding, C. J. Summers and Z. L. Wang, "Large-scale synthesis of six-nanometer-wide ZnO nanobelts", ***The Journal of Physical Chemistry B***, 108 (26), 8773-8777 (2004).
57- G. Williams and P. V. Kamat, "Graphene-semiconductor nanocomposites: excited-state interactions between ZnO nanoparticles and graphene oxide", ***Langmuir***, 25 (24), 13869-13873 (2009).
58- J. Zhang, J. Wang, S. Zhou, K. Duan, B. Feng, J. Weng and P. Wu, "Ionic liquid-controlled synthesis of ZnO microspheres", ***Journal of Materials Chemistry***, 20 (43), 9798-9804 (2010).
59- M. H. Kahsay, A. Tadesse, D. RamaDevi, N. Belachew and K. Basavaiah, "Green synthesis of zinc oxide nanostructures and investigation of their photocatalytic and bactericidal applications", ***RSC Advances***, 9 (63), 36967-36981 (2019).
60- M. S. Ghamsari, S. Alamdari, D. Razzaghi and M. A. Pirlar, "ZnO nanocrystals with narrow-band blue emission", ***Journal of Luminescence***, 205, 508-518 (2019).
61- H. Sowa and H. Ahsbahs, "High-pressure X-ray investigation of zincite ZnO single crystals using diamond anvils with an improved shape", ***Journal of Applied Crystallography***, 39 (2), 169-175 (2006).
62- M. Dutta, S. Mridha and D. Basak, "Effect of sol concentration on the properties of ZnO thin films prepared by sol–gel technique", ***Applied Surface Science***, 254 (9), 2743-2747 (2008).
63- M. F. Al-Hakkani, G. A. Gouda, S. H. Hassan and A. M. Nagiub, "Echinacea purpurea mediated hematite nanoparticles (α-HNPs) biofabrication, characterization, physicochemical properties, and its in-vitro biocompatibility evaluation", ***Surfaces and Interfaces***, 24, 101113 (2021).
64- S. H. Abdel-Halim, A. M. A. Shehata and M. F. El-Shahat, "Removal of lead ions from industrial wastewater

by different types of natural materials″, **Water Research**, 37 (7), 1678-1683 (2003).
65- Y. H. Li, S. Wang, J. Wei, X. Zhang, C. Xu, Z. Luan and B. Wei, ″Lead adsorption on carbon nanotubes″, ***Chemical Physics Letters***, 357 (3-4), 263-266 (2002).
66- A. E. Burakov, E. V. Galunin, I. V. Burakova, A. E. Kucherova, S. Agarwal, A. G. Tkachev and V. K. Gupta, ″Adsorption of heavy metals on conventional and nanostructured materials for wastewater treatment purposes: A review″, ***Ecotoxicology and Environmental Safety***, 148, 702-712 (2018).
67- M. Erhayem, F. Al-Tohami, R. Mohamed and K. Ahmida, ″Isotherm, kinetic and thermodynamic studies for the sorption of mercury (II) onto activated carbon from Rosmarinus officinalis leaves″, ***American Journal of Analytical Chemistry***, 6 (01), 1 (2015).
68- Y. C. Lee and J. W. Yang, ″Self-assembled flower-like TiO_2 on exfoliated graphite oxide for heavy metal removal″, ***Journal of Industrial and Engineering Chemistry***, 18 (3), 1178-1185 (2012).
69- L. Fan, C. Luo, M. Sun, X. Li and H. Qiu, ″Highly selective adsorption of lead ions by water-dispersible magnetic chitosan/graphene oxide composites″, ***Colloids and Surfaces B: Biointerfaces***, 103, 523-529 (2013).
70- A. Z. M. Badruddoza, Z. B. Z. Shawon, M. T. Rahman, K. W. Hao, K. Hidajat and M. S. Uddin, ″Ionically modified magnetic nanomaterials for arsenic and chromium removal from water″, ***Chemical Engineering Journal***, 225, 607-615 (2013).
71- L. Hao, H. Song, L. Zhang, X. Wan, Y. Tang and Y. Lv, ″SiO_2/graphene composite for highly selective adsorption of Pb (II) ion″, ***Journal of Colloid and Interface Science***, 369 (1), 381-387 (2012).
72- G. Yin, X. Song, L. Tao, B. Sarkar, A. K. Sarmah, W. Zhang and H. Wang, ″Novel Fe–Mn binary oxide-biochar as an adsorbent for removing Cd (II) from aqueous solutions″, ***Chemical Engineering Journal***, 389, 124465 (2020).
73- Y. K. Penke, G. Anantharaman, J. Ramkumar and K. K. Kar, ″Aluminum substituted cobalt ferrite (Co–Al–Fe) nano adsorbent for arsenic adsorption in aqueous systems and detailed redox behavior study with XPS″, ***ACS Applied Materials & Interfaces***, 9 (13), 11587-11598 (2017).
74- T. Liu, Y. Li, Q. Du, J. Sun, Y. Jiao, G. Yang, Z. Wang, Y. Xia, W. Zhang and D. Wu, ″Adsorption of methylene blue from aqueous solution by graphene″. ***Colloids and Surfaces B: Biointerfaces***, 90, 197-203 (2012).
75- Y. Ren, N. Yan, Q. Wen, Z. Fan, T. Wei, M. Zhang and J. Ma, ″Graphene/δ-MnO_2 composite as adsorbent for the removal of nickel ions from wastewater″, ***Chemical Engineering Journal***, 175, 1-7 (2011).
76- G. A. Gouda, M. Shatat, T. Seaf elnasr and M. Abdallah, ″Potentiometric and thermodynamic investigation of rhenium (V) complexes with 1-methyl-2-mercaptoimidazole″, ***Al-Azhar Bulletin of Science***, 24 (2-A), 141-148 (2013).
77- A. A. Amindzhanov, K. A. Manonov, N. G. Kabirov and G. A. H. Abdelrahman, ″Copper (II) complexation with 1-methyl-2-mercaptoimidazole in 7 M HCl″. ***Russian Journal of Inorganic Chemistry***, 61 (1), 81-85 (2016).

Bull. Pharm. Sci., Assiut University, Vol. 45, Issue 1, 2022, pp. 23-40

نشـرة العلـوم الصيدليـــــة
جامعة أسيوط

BULL. PHARM. SCI. Assiut Univ.

تحضير حبيبات اكسيد الزنك النانوية باستخدام بولي إيثيلين جليكول بطريقة تحكم الميكروويف

عبدالهادي سليمان عبد الهادي[١] – جمال عبدالعزيز جودة[١] – عبدالرحمن مصطفي حامد[١] – محمد عبدالرحيم أبو سعيد[٢] – محمد عبدالمطلب[١]

[١] قسم الكيمياء ، كلية العلوم ، جامعة الأزهر ، فرع أسيوط ، أسيوط ٧١٥٢٤ ، مصر

[٢] معهد بحوث التكنولوجيا المتقدمة والمواد الجديدة ، مدينة البحث العلمي والتطبيقات التكنولوجية ، برج العرب الجديدة ، الإسكندرية ٢١٩٣٤ ، مصر

تم تحضير جسيمات أكسيد الزنك النانوية (ZnO NPs) باستخدام بعض العوامل المؤثرة مثل البولي إيثيلين جلايكول (PEG) كعامل تثبيت عند درجة حموضة ودرجات حرارة مختلفة. كانت أفضل الظروف لتحضير أكسيد الزنك النانوية عند درجة الحموضة (pH) هي ١١ وتركيز ٠,١ مولر (٧,٥ مل) من البولي إيثيلين جلايكول مع وزن جزيئي ٢٠٠٠٠ ودرجة حرارة ٦٠ درجة مئوية. تم تأكيد خصائص أكسيد الزنك النانوية المُحضرة باستخدام تقنيات مختلفة مثل الاشعة تحت الحمراء (FTIR) ، والتحليل الطيفي الشامل (UV-Vis) ، حيود الأشعة السينية (XRD) والماسح المجهري الإلكتروني (SEM) والمجهر الإلكتروني النافذ (TEM). من الواضح أن طيف (UV-Vis) لـــ أكسيد الزنك النانوية أظهر ذروة امتصاص عند ٢٦٨ و ٣٦٢ نانومتر مع فجوة نطاق مباشرة تبلغ ٣,٣٩ فولت. ظهرت باستخدام مطياف اللمعان الضوئي (PL) لاكسيد الزنك النانوية ذروة انبعاث عند ٤٢٠ نانومتر. كان متوسط الأحجام المحسوبة لحبيبات أكسيد الزنك النانوية باستخدام طريقة توسيع الخط في(XRD) ١٩,٧١ نانومتر. أظهرت تحاليل المجهر النافذ للضوء (TEM) أن أكسيد الزنك النانوية المحضرة كروية بأقطار مختلفة في المدى ٢٢,٢ – ٢٧,٨ نانومتر. علاوة على ذلك ، فإن أكسيد الزنك النانوية المحضرة لديها قدرة امتصاص ممتازة لإزالة بعض الكاتيونات من الماء. كانت سعات الامتزاز ٣٩١,٦ و ٤٣٧,٢ مجم / جم لكل من Mn (II) و Cd (II) على التوالي. سيتم وصف نماذج لانجمير (Langmuir) و فروندليش (Freundlich) و تامكين (Temkin) جيدًا لعملية الامتزاز. من الناحية الديناميكية الحرارية ، كانت عمليات امتصاص اكسيد الزنك النانوية تلقائية وماصة للحرارة وذات طبيعة فيزيائية. تشير كفاءة إزالة ايونات Mn (II) و Cd (II) الجيدة بواسطة أكسيد الزنك النانوية و قدرتها الاستثنائية على الامتصاص إلى أن أكسيد الزنك النانوية ممكن يكون لها تطبيقات محتملة كبيرة في حماية البيئة.